Effect of Precipitate Characteristics on the Corrosion Behavior of a AZ80 Magnesium Alloy

Dhananjay Dubey[1] · **Kondababu Kadali**[1] · **Harikrishna Kancharla**[1] · **Anuz Zindal**[2] · **Jayant Jain**[2] · **K. Mondal**[1] · **Sudhanshu S. Singh**[1]

Abstract

In this study, a systematic investigation on the effect of both aging temperature (250 °C and 330 °C) and time (chosen based on aging curves) on the distribution and volume fraction of the $Mg_{17}Al_{12}$ precipitates and subsequently on the corrosion behavior of the AZ80 magnesium alloy was carried out by conducting both immersion and dynamic polarization test in a freely aerated 3.5% NaCl solution. The analysis of corrosion products using Raman spectroscopy and X-ray diffraction and investigation of corrosion morphologies using scanning electron microscopy suggested galvanic corrosion of the anodic α-Mg matrix in contact with the cathodic $Mg_{17}Al_{12}$ precipitates. The higher corrosion resistance of the alloy aged at lower temperature (250 °C) was attributed to the higher number density of the $Mg_{17}Al_{12}$ precipitates than that at higher temperature (330 °C). In the peak aged condition, the average number densities of precipitates ($1/\mu m^2$) were measured to be ~0.74 and ~0.32 and average corrosion rates (mm/y) were measured to be ~3.0 and ~5.0 at the aging temperatures of 250 °C and 330 °C, respectively. At a particular aging temperature, the corrosion resistance increased to a maximum at peak-aged condition followed by a decline in the over-aged condition and further increase with prolong aging, which was correlated with the number density, size and distribution of the $Mg_{17}Al_{12}$ precipitates.

Keywords AZ80 magnesium alloy · Aging · $Mg_{17}Al_{12}$ · Corrosion · Electron microscopy

1 Introduction

Magnesium alloys have the potential to be used in automobile, aerospace, and electronic sectors because of their excellent properties, such as castability, high specific strength, and good damping ability [1]. However, lack of the room temperature ductility and high susceptibility to corrosion limit their applicability [2]. Among various magnesium alloys, the AZ series (magnesium–aluminum–zinc) alloys, in particular, the AZ80, have gained interest over the years. As the solubility of aluminum in the AZ series magnesium alloys decreases with the decrease in temperature, they can be precipitation hardened by performing high temperature aging [3–5]. The microstructure of an aged magnesium alloy consists of α-Mg matrix and $Mg_{17}Al_{12}$ precipitates. The distribution and volume fraction of the precipitate depend upon the aging temperature and time [4, 5].

The $Mg_{17}Al_{12}$ precipitates have been reported to affect the corrosion behavior of the AZ series magnesium alloys [6–9]. For instance, Song et al. [6] observed the presence of $Mg_{17}Al_{12}$ precipitates during aging increases the corrosion resistance as compared to the as-cast AZ91 magnesium alloy. Fukuzaki et al. [7] also indicated that the $Mg_{17}Al_{12}$ precipitates act as barrier and decrease the corrosion resistance of AZ91 alloy after aging. Further, the work of Song et al. [8] discussed the dual role of the $Mg_{17}Al_{12}$ precipitates on the corrosion response and observed that the corrosion rate of the as-cast AZ91D magnesium alloy first decreases followed by an increase with the aging time at a constant temperature of 160 °C. Raman et al. [9] observed a decrease in the corrosion resistance of AZ91 alloy with increase in aging time at aging temperature of 200 °C and attributed this behavior to the increase in the ratio of the $Mg_{17}Al_{12}$ phase to the α-Mg phase. Zhao et al. [10] investigated the role of different morphologies of the $Mg_{17}Al_{12}$ phase on the

✉ Sudhanshu S. Singh
sudhanss@iitk.ac.in

1 Department of Materials Science and Engineering, Indian Institute of Technology Kanpur, Kanpur, UP 208016, India

2 Department of Materials Science and Engineering, Indian Institute of Technology Delhi, New Delhi 110016, India

Table 1 Chemical composition of AZ80 magnesium alloy measured by OES

Elements	Al	Zn	Mn	Si	Fe	Mg
wt%	9.1	0.45	0.15	0.025	0.007	Remaining

corrosion behavior of the AZ91 alloy. Li et al. [11] have compared the corrosion behavior of the as-cast, peak-aged and homogenized AZ63 magnesium alloys, where the T4 condition possesses the lowest corrosion resistance. Among the as-cast, solutionized and aged AZ61 alloys, Dai et al. [12] observed that the corrosion resistance of solutionized AZ61 was the lowest at the same impurity level (Fe content) and attributed this to be due to the dissolution of $Mg_{17}Al_{12}$ precipitates.

Only a handful of studies [13, 14] have reported the effect of $Mg_{17}Al_{12}$ precipitates on the corrosion behavior of the AZ80 magnesium alloy. Liao et al. [13] have studied the effect of aging time at 170 °C on the corrosion behavior of the as-forged AZ80 magnesium alloy. A decrease in the corrosion rate at the initial stage of aging followed by an increase in the corrosion rates at the later stage was observed. In another study by Zeng et al. [14], the effect of T5 treatment (177 °C for 16 h) on the corrosion behavior of an extruded AZ80 alloy has been investigated, where the network of the $Mg_{17}Al_{12}$ phase along the grain boundaries has been attributed to the observed pitting and intergranular corrosion (IGC).

The above findings suggest that the $Mg_{17}Al_{12}$ phase has a critical role in determining the corrosion behavior, and any change in the distribution of this phase would result in a dramatic change in the corrosion resistance of the magnesium alloys. Although studies have been conducted to understand the effect of the $Mg_{17}Al_{12}$ precipitates on the corrosion behavior of aged magnesium alloys [13, 14], most of them have been performed at lower aging temperatures (< 200 °C). Further, a systematic investigation on the effect of both aging temperature and time on the microstructure and subsequently on the corrosion response has not been carried out, and hence it needs attention. This is important as the distribution and volume fraction of the $Mg_{17}Al_{12}$ precipitates depend on both the aging temperature and time.

Hence, in this work, the effect of higher aging temperatures (250 °C and 330 °C) and durations (chosen based on the aging curve) on the microstructure, and subsequently the effect of microstructure on the corrosion behavior of a AZ80 magnesium alloy have been investigated by conducting immersion and dynamic polarization test in a freely aerated 3.5% NaCl solution.

Table 2 Selected aging temperatures and durations for the evaluation of corrosion behavior of the AZ80 alloy

Aging temp./time	250 °C	330 °C
4 h	Under-aged	Under-aged
8 h	NA	Peak-aged
16 h	Peak-aged	Over-aged
30 h	Over-aged	Over-aged
48 h	Highly over-aged	Highly over-aged
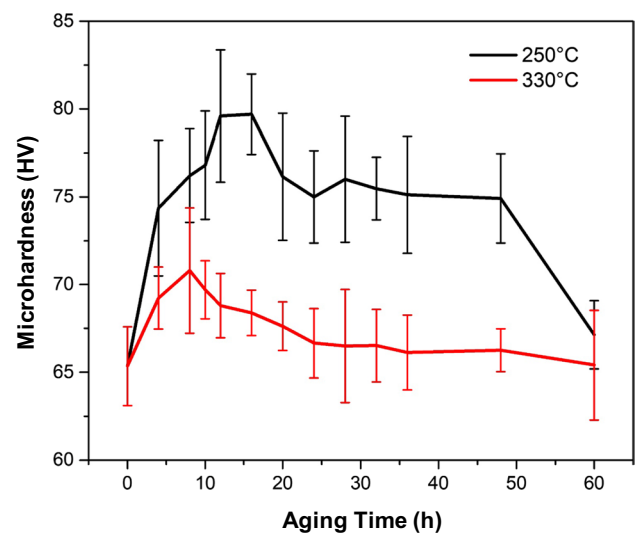
Fig. 1 Aging curve of the AZ80 magnesium alloy at 250 °C and 330 °C [5]

2 Experimental Methods

2.1 Initial Alloy and Heat-Treatment

As-cast AZ80 magnesium alloy was used as a starting material. The nominal chemical composition of the alloy, measured by optical emission spectroscopy (OES), is provided in Table 1. These as-cast samples were first solutionized at 390 °C for 24 h, then quenched in water and finally aged at 250 °C and 330 °C for different durations, as listed in Table 2. The aging temperatures and durations were chosen to cover all the aging conditions at a particular temperature, i.e., under-aged, peak-aged and over-aged. The aging curves of the AZ80 alloy at 250 °C and 330 °C, obtained in our previous study, are shown in Fig. 1 [5].

2.2 Microstructural Characterization

For microstructural characterization using a scanning electron microscope (SEM, Carl Zeiss EVO 50), samples were first polished till 0.05 μm alumina solution. At every polishing step, ethanol was used instead of water to avoid corrosion of the samples while polishing. Finally, these polished samples were ultrasonically cleaned in ethanol solution for 7–8 min followed by etching in a 10% Nital solution.

2.3 Corrosion Tests

To perform the immersion and potentiodynamic polarization tests, samples (15 mm × 15 mm × 5 mm) were cut from the ingot using wire electric discharge machining (EDM) and polished using the procedure mentioned above.

2.3.1 Immersion Test

Except for one polished surface, all other surfaces of the samples were first covered with the paint (lacquer) and then with the Teflon tape. The samples were then completely immersed into a freely aerated 3.5% NaCl solution for 7 days with the help of wires, which were also covered with the paint and the Teflon tape to avoid the formation of a galvanic couple between the sample and wire. For each condition, at least three samples were exposed to check the repeatability. After exposure, samples were immersed in chromate acid (200 g/L CrO_3 + 10 g/L $AgNO_3$) [13] at room temperature for ~ 7–8 min to remove the corrosion products. The samples were then cleaned with tap water, dried with blower and weighted to measure the weight loss. Corrosion rates were calculated from the measured weight loss by using the formula provided in ASTM G1-03 [15]:

$$\text{Corrosion rate(mm/y)} = \frac{\Delta W}{(A \times \rho \times t)} \times 8.76 \times 10^4 \qquad (1)$$

where, A is the exposed area in cm^2, ΔW is the weight loss in g, ρ is the density of each alloy in g/cm^3, and t is the immersion time in h.

2.3.2 Electrochemical Test

Potentiodynamic polarization tests were conducted by using PARSTAT 2263 Model potentiostat (Princeton Applied Research, USA) as per the ASTM standard (G3-14) in a freely aerated 3.5% NaCl solution [16]. The samples were polished using the same procedure till the final polishing of 0.05 μm alumina followed by cleaning in an ultrasonicator for 10 min followed by air drying. The NaCl solution was kept in an electrochemical cell consisting of a standard

three electrode system. The saturated calomel electrode and a platinum mesh were used as the reference electrode and counter electrode, respectively. An area of 1 cm^2 of the sample was exposed to the solution in a standard flat bottom cell. Polarization tests were performed at a scan rate of 0.5 mV/s in cathodic and anodic ranges of OCP − 250 mV and OCP + 1000 mV, respectively. For each condition, at least three tests were conducted to check the repeatability. The corrosion rate was calculated according to the following formula [17]:

$$\text{Corrosion rate(mm/y)} = 3.27 \times 10^{-3} \times \frac{i_{\text{corr}}}{\rho} \times \text{EW} \qquad (2)$$

where, EW and ρ are the equivalent weight (g) and density of the alloy (g/cm^2), respectively. i_{corr} is the current density ($\mu A/cm^2$) which is measured using Tafel extrapolation method [16].

2.4 Post Corrosion Characterization

To understand the corrosion mechanism, both the cross-section and top surface of the corroded samples were observed using a scanning electron microscope (Carl Zeiss EVO 50). Corrosion products were investigated using X-ray diffraction (XRD) followed by Raman spectroscopy after immersion tests. XRD (Panalytical XPert) was carried out using a Cu (Kα) radiation at a scan rate of 2°/minute in the range of 10°–90°. The Raman spectroscopy (LabRam HR800) was conducted at a range of 200–2700 cm^{-1}.

3 Results and Discussion

The backscattered electron (BSE) images of the cast and the solutionized AZ80 alloy are shown in Fig. 2a and b, respectively. The as-cast microstructure contains α-Mg (matrix) and two second phase particles, which are eutectic $Mg_{17}Al_{12}$ and Al_8Mn_5 particles shown by arrows. Due to the difference in the contrast, both the second phase particles are clearly visible in the BSE image (Fig. 2a). The white particles are Al_8Mn_5 type, while the gray particles are the $Mg_{17}Al_{12}$ type. The compositions of these particles are provided in Table 3. The compositions of the second phase particles were measured by EDS (energy dispersive spectroscopy) using the procedure mentioned in [18, 19]. These particles have also been reported in the previous studies [18, 20, 21]. Further, it is evident from Fig. 2b that the $Mg_{17}Al_{12}$ eutectic precipitates dissolved during solution heat treatment, whereas, the Al_8Mn_5 particles were still present. This could be attributed to the fact that Al_8Mn_5 particles do not dissolve into the matrix and are stable at the solutionization temperature as used here [22, 23].
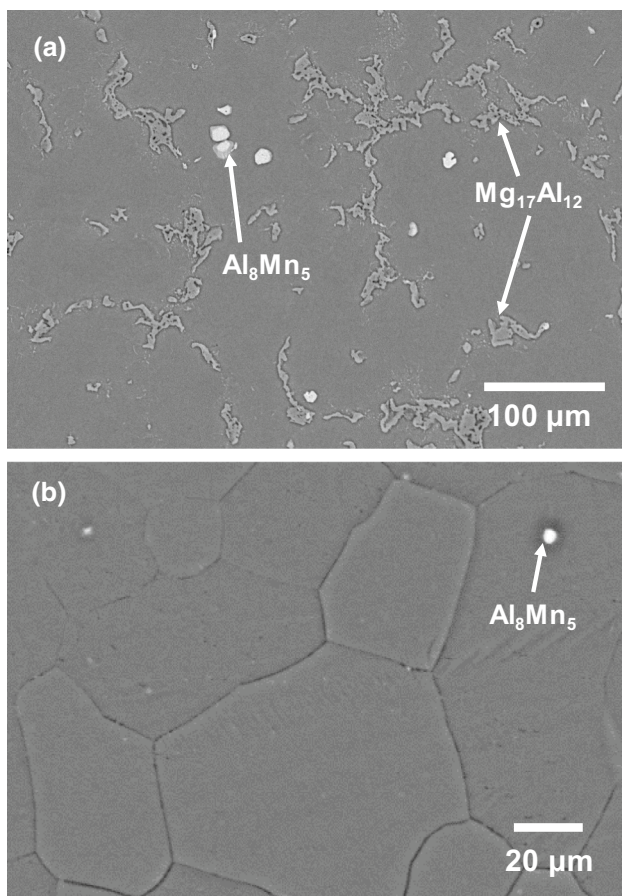
Fig. 2 BSE images of **a** as-cast and **b** solutionized at 390 °C for 24 h AZ80 magnesium alloy

Figure 3 shows a typical representative microstructure of the AZ80 magnesium alloy after aging treatment (250 °C, 4 h), where the $Mg_{17}Al_{12}$ particles formed due to precipitation from the supersaturated matrix can be observed. Figure 3 also indicates different microstructural features formed due to aging, namely continuous and discontinuous precipitates; grain boundary precipitates; and precipitates free zone (PFZs). Depending on the way these precipitates form, they can be predominately divided into two categories: continuous and discontinuous [24]. Discontinuous precipitates are formed from the grain boundaries, as shown by the arrows in Fig. 3. It has been shown in the previous studies that discontinuous precipitation is favored over continuous precipitation when the grain boundary diffusion is dominant, whereas the continuous precipitation is favored when volume diffusion is dominant [25]. Further, the formation of discontinuous and continuous

precipitates has been found to be preferred at lower and higher aging temperatures, respectively [25, 26]. At the intermediate temperatures, both discontinuous and continuous precipitates are formed. Figure 3 also shows grain boundary precipitates and precipitate free zones (PFZs). As the precipitation process is related to diffusion, the size, distribution and volume fraction of the $Mg_{17}Al_{12}$ precipitates depend upon both the aging temperature and time. On the basis of general observations in Fig. 3, detailed analysis of the microstructure of the alloy at two different aging temperatures with varying durations has been carried out.

Figure 4a–d and e–i show the microstructures of the alloy after aging treatment at 250 °C and 330 °C for different durations as mentioned in Table 1, respectively. Qualitatively, as temperature increases from 250 to 330 °C, the size of the precipitates inside the grains as well as the distance between the neighboring precipitates appear to increase. It suggests that the number density of the precipitates (number per unit area) decreases with increase in temperature. Furthermore, the extent of discontinuous precipitation decreases as the temperature is raised from 250 to 330 °C. For the case of sample aged at 250 °C-4 h (Fig. 4a), the microstructure contains both the discontinuous lamellar $Mg_{17}Al_{12}$ precipitates along with the continuous precipitates. However, at higher temperature (330 °C), the precipitation nature is predominantly continuous. The size of the PFZ and grain boundary precipitates also tend to increase with an increase in both the aging temperature and time. A similar trend for the grain boundary precipitates and PFZ has been observed in the previous study on the same alloy [5].

Figure 5 shows the variation of number density of the precipitates inside the grains with aging conditions. At least one thousand precipitates were taken into consideration to obtain the number densities. The number density of the precipitates increases with the aging time at 250 °C and reaches to a maximum at 16 h (Fig. 4b), which also corresponds to the peak-aged condition at 250 °C. After 16 h of aging, the number density of precipitates decreases and then remains almost constant even at highly overaged condition. A similar trend was observed at 330 °C, where the precipitate density first reaches to a maximum at 8 h followed by a decrease in over-aged condition and finally remains almost constant with the prolong aging. It should be noted that the highest number density of the precipitates is associated with the peak-aged condition for both the aging temperatures.

The corrosion rates, calculated from the measured weight loss during immersion tests, at different aging temperatures

Table 3 Compositions (at%) of the second phase particles in as-cast AZ80 magnesium alloy

Elements	Mg	Al	Zn	Mn	Fe
White particles	–	59.16 ± 0.87	–	39.22 ± 1.30	0.51 ± 0.45
Gray particles	60.19 ± 0.51	38.69 ± 0.52	01.8 ± 0.03	–	–

Fig. 3 SEM micrograph of an aged alloy (250 °C, 4 h) illustrating the typical distribution of precipitates post aging
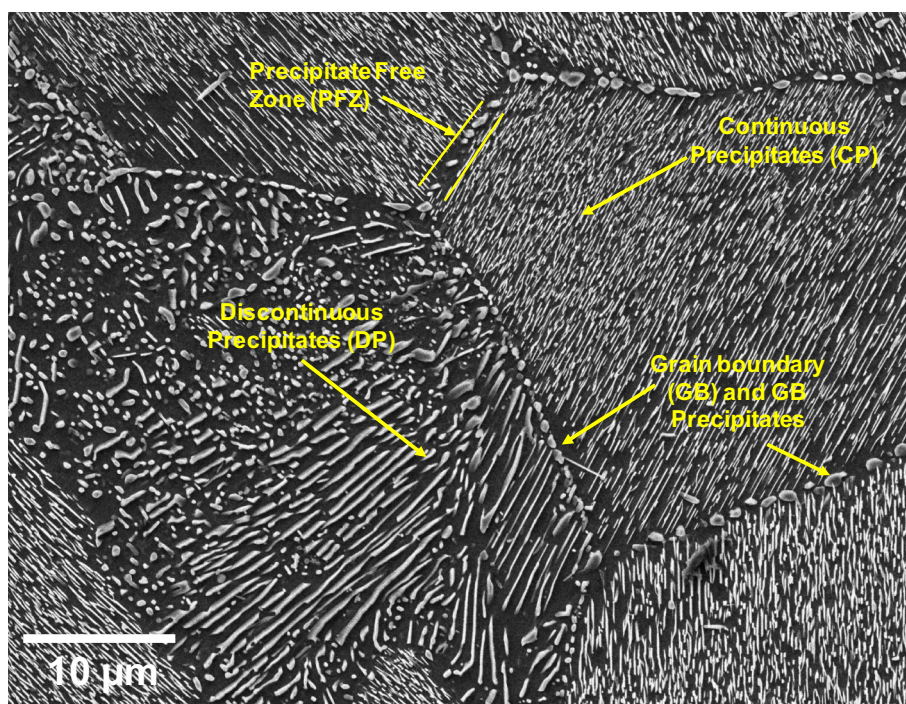

and durations, are shown in Fig. 6. For comparison, the corrosion rate data for the solutionized condition has also been included. It can be observed that all the aged conditions are better corrosion resistant than the solutionized condition. The alloys aged at 250 °C were found to be more corrosion resistant than the alloys aged at 330 °C. At both the aging temperatures, the corrosion rate first decreases with aging time followed by an increase in the over-aged condition. However, the prolong aging (highly over-aged) results in further decrease in corrosion rate. The maximum corrosion resistance in both aging temperatures corresponds to the peak-aged conditions. A similar trend of decreasing corrosion rate with an increase in the aging time during initial aging, at lower aging temperatures, has also been observed in the as-cast AZ91 [6] and as-forged AZ80 magnesium alloys [13]. However, in both the studies the corrosion rates continue to increase with extended aging time as opposed to the observed decrease in the corrosion rates at the later stage of aging (highly over-aged) in the present study. The observed trends in the corrosion resistance of the alloy can be attributed to the distribution of $Mg_{17}Al_{12}$ and aluminum content in the matrix, which will be discussed in the later section.

Electrochemical tests were conducted only on the peak-aged and the over-aged conditions, i.e., 250 °C-16 h, 250 °C-30 h, 330 °C-8 h and 330 °C-30 h. Figure 7a shows the polarization curves for these aging conditions. At both the aging temperatures, the curves moved toward more negative potential and to the right with an increase in aging time, indicating peak-aged conditions to be more corrosion

resistant than the over-aged conditions. Similarly, with an increase in aging temperature from 250 to 330 °C at a constant aging time of 30 h, the curve moves towards the right indicating that increasing the aging temperature leads to the decrease in the corrosion resistance. The corrosion rates for both the peak-aged and the over-aged conditions, at both the temperatures, have been shown in Fig. 7b. These results corroborate with the results obtained from the immersion tests and confirm that the peak-aged conditions exhibit the highest corrosion resistance.

In chloride solution, the $Mg_{17}Al_{12}$ phase has been observed to be cathodic with respect to the matrix [18]. According to Song et al. [6, 8], the corrosion resistance of magnesium alloys depends upon the distribution and volume fraction of $Mg_{17}Al_{12}$ phases in the alloy. If the volume fraction of $Mg_{17}Al_{12}$ phases is low and their network is disrupted (not continuous) then the $Mg_{17}Al_{12}$ acts as a local galvanic couple and the corrosion resistance decreases. However, if the volume fraction is high then these phases will form a continuous network, acting as a barrier, resulting in the increase in the corrosion resistance of the alloy. In this study, after aging, the volume fraction of the $Mg_{17}Al_{12}$ phase is in the higher regime and they form continuous networks (Fig. 4), as opposed to the as-cast microstructure where the volume fraction of the $Mg_{17}Al_{12}$ is in the lower regime. Therefore, the $Mg_{17}Al_{12}$ phase in the aged conditions is expected to increase the overall corrosion resistance of the alloy in contrast to the observed decrease in the corrosion resistance of the as-cast alloy from the solutionized condition, as reported in our previous study [18]. Furthermore,

Fig. 4 SEM images of the AZ80 alloy after aging. **a–d** are at 250 °C for 4 h, 16 h, 30 h, 48 h, respectively and **e–i** are at 330 °C for 4 h, 8 h, 16 h, 30 h, 48 h, respectively
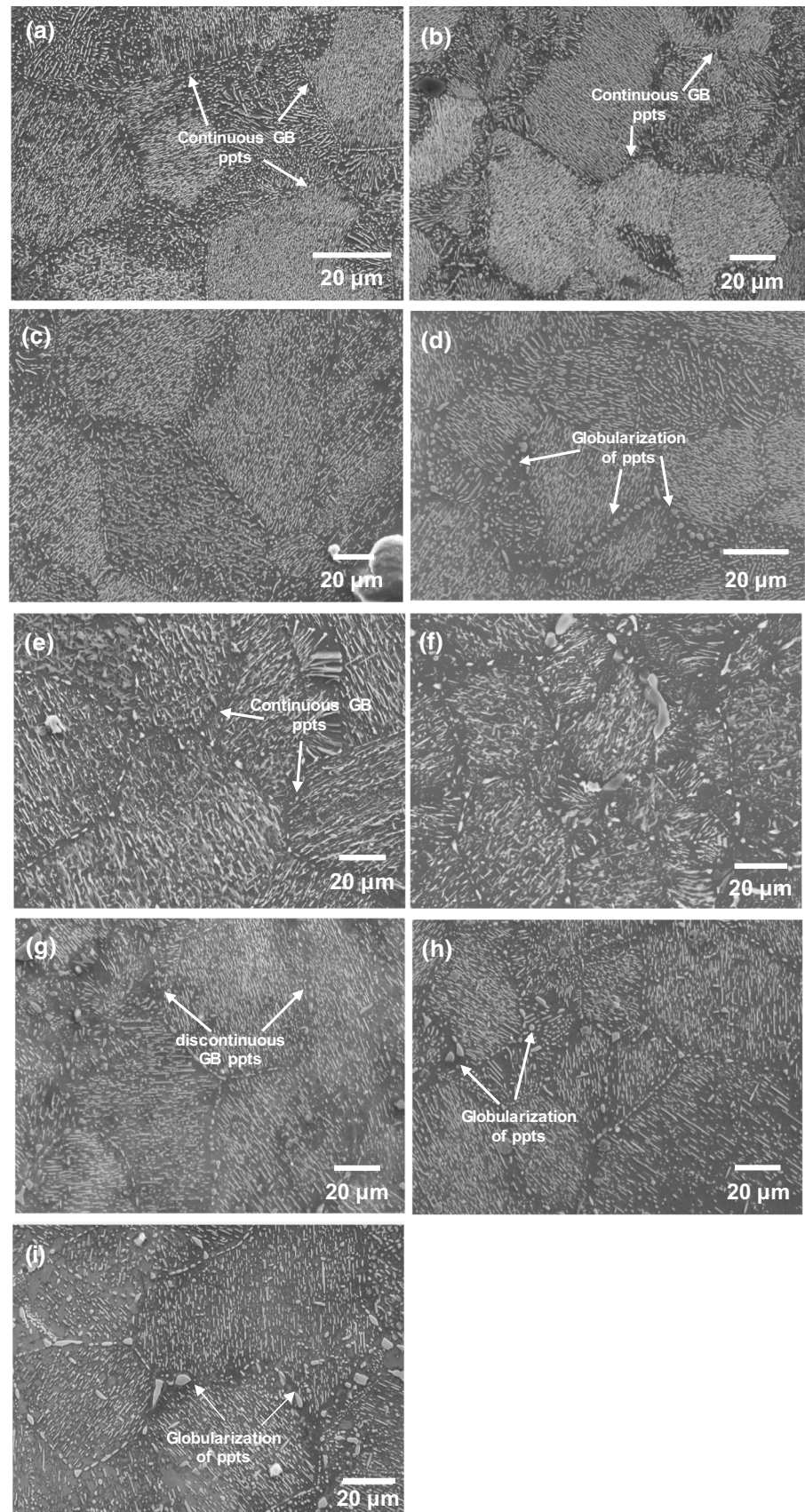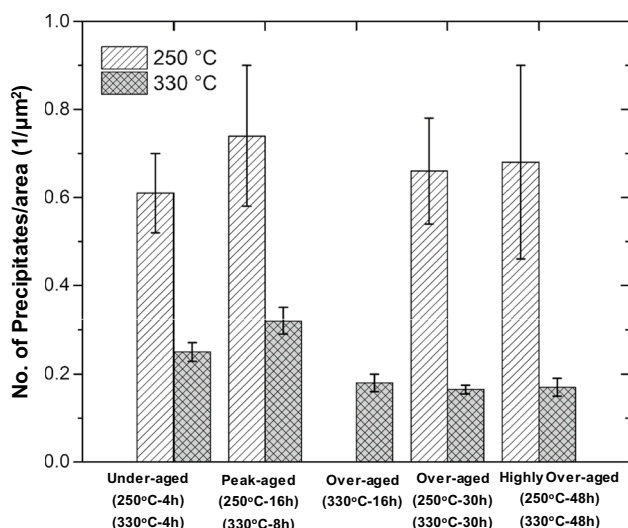
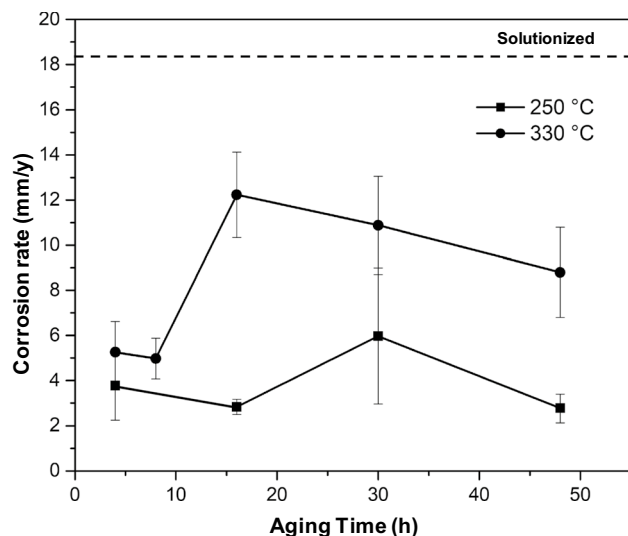**Fig. 5** Variation of number density of precipitates with different aging conditions

Fig. 6 Corrosion rates at different aging temperatures and times from immersion tests. For comparison, solutionized condition has also been included

apart from the microstructural changes (Fig. 4), the aluminum concentration in the α-Mg also changes with the aging time. The precipitation of the $Mg_{17}Al_{12}$ results in the decrease in aluminum concentration in the matrix and this could lead to the manifestation of decrease in the corrosion resistance of the matrix. In summary, two competitive mechanisms would determine the corrosion resistance of the AZ80 magnesium alloy in the aged conditions: (a) increase in the corrosion resistance of the alloy due to the formation of a continuous network of $Mg_{17}Al_{12}$ precipitates, and (b) decrease in the corrosion resistance due to decrease in
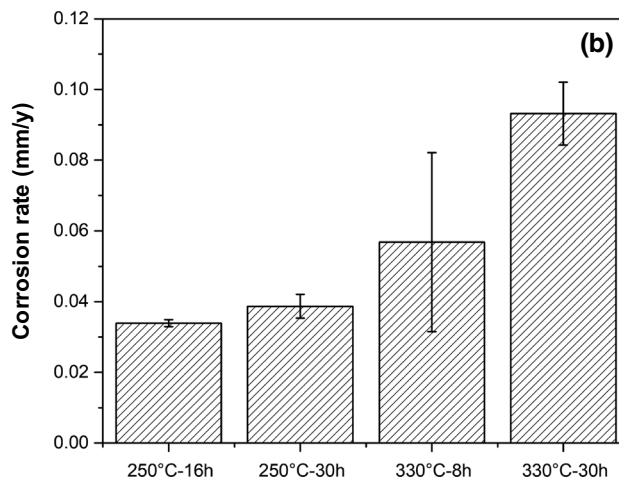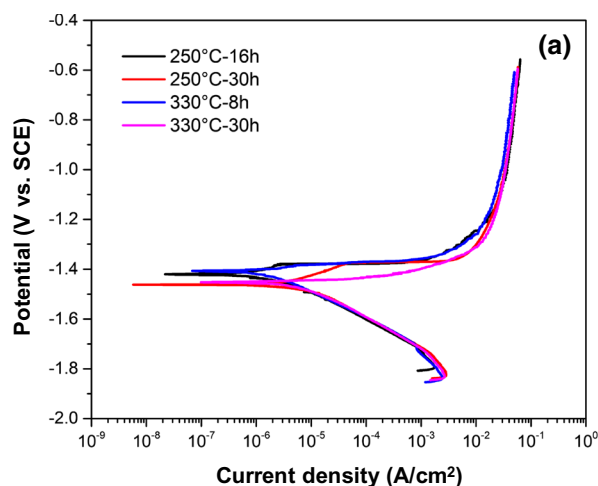
Fig. 7 **a** Polarization curves and **b** corrosion rates for different aging conditions from electrochemical tests

aluminum concentration of matrix owing to the formation of precipitates. These two competing mechanisms will also be influenced by the inherent galvanic coupling between the precipitate and the matrix with depleted Al as well as the morphology, size and number density of the precipitates in the matrix as well as along the grain boundary.

Figure 8a, b and c, d show the SEM images of the top surfaces of the 250 °C-48 h and 330 °C-15 h, respectively, after corrosion. Figure 8e, f shows the SEM image of the cross-section of the 250 °C, 15 h. Figure 8b, d, and f are the magnified versions of the selected areas (red rectangles) in Fig. 8a, c, and e, respectively. It is to be noted that the corroded samples have been cleaned before taking these images. All these images clearly reveal the dissolution of the α-Mg matrix leaving behind the $Mg_{17}Al_{12}$ precipitates (shown by arrows) due to the formation of local galvanic couples and micro-galvanic effect. Furthermore, this also suggests that the corrosion proceeds with the dissolution of the matrix between precipitates and would inhibit as soon as
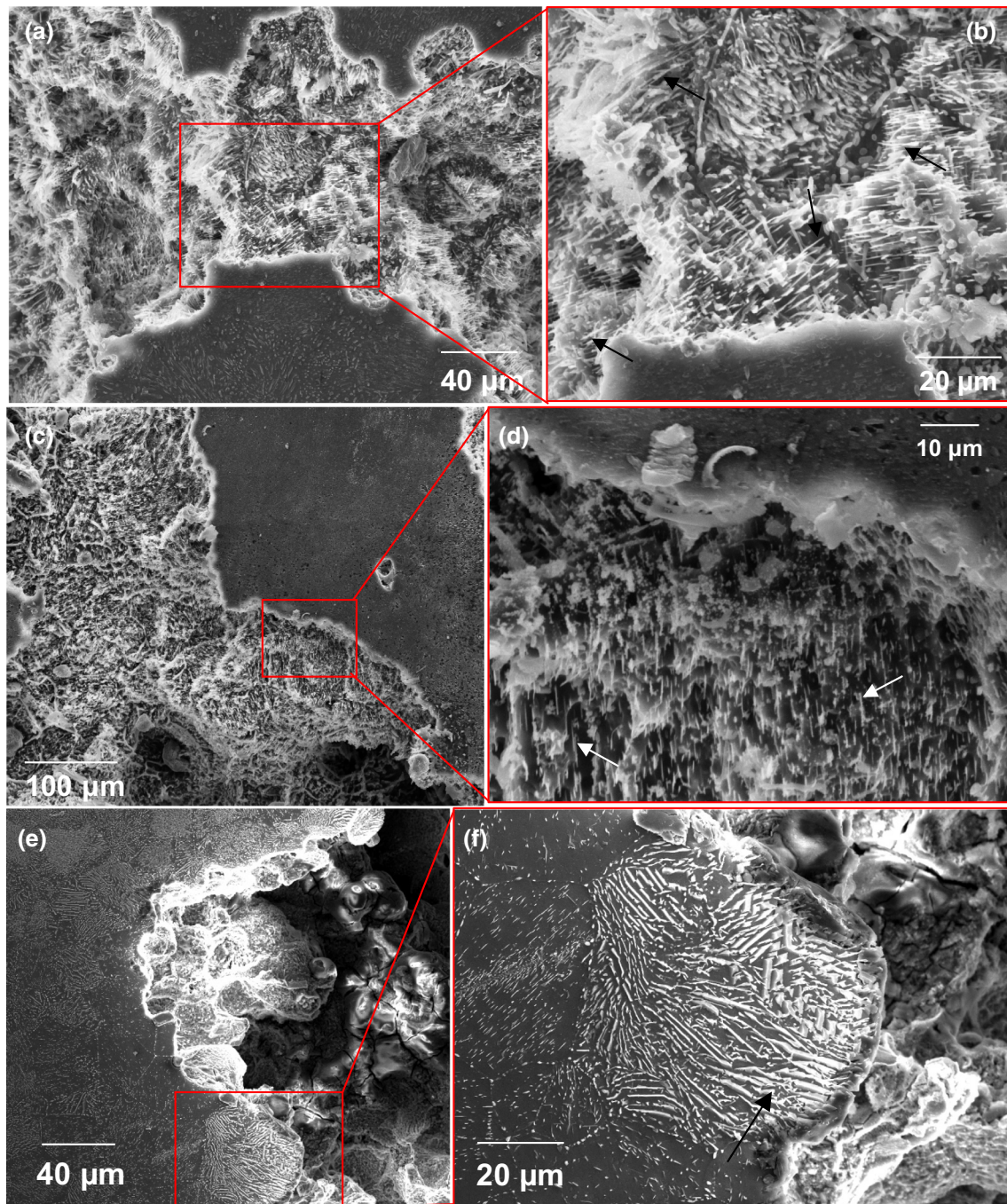
Fig. 8 SEM images of aged alloy after corrosion: top surfaces **a**, **b** 250 °C, 48 h, **c**, **d** 330 °C, 16 h and cross-section **e**, **f** 250 °C, 16 h

more corrosion resistant $Mg_{17}Al_{12}$ precipitates would come in contact with the corrosion front, the probability of which is higher when the network is highly continuous, i.e., when the number density of precipitates is high. This is clearly visible in Fig. 8e, where the corrosion has slowed down when it approaches the area of high density of precipitates (a continuous network inside red rectangle) as opposed to the other area of the sample, where the precipitate density is lower.

The increase in number density with the aging time is clearly visible for both the temperatures in Fig. 5 till the peak aging. Interestingly, with the increase in number density, the corrosion rate has also decreased suggesting the cohesiveness with the mechanism as stated here.
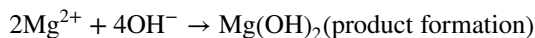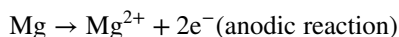
The observed increase in the corrosion resistance in the aged conditions at both 250 °C and 330 °C (Fig. 6) compared to the solutionized condition is attributed to the

presence of high number density and continuous $Mg_{17}Al_{12}$ precipitates in the aged conditions. Also, the higher number density of the $Mg_{17}Al_{12}$ precipitates in 250 °C aged alloy than in 330 °C aged results in the observed higher corrosion resistance of the samples aged at 250 °C. In both the cases, the presence of large number density of cathodic precipitates appears to dominate over the negative effect of the matrix with the depleted aluminum towards corrosion. It is interesting to note that the trend of corrosion rates (Fig. 6) at a particular temperature also follows the observed trend for the precipitate density (Fig. 5). The observed lowest corrosion rates in the peak-aged conditions at both the aging temperatures have resulted from the highest number densities of the $Mg_{17}Al_{12}$ precipitates.

The increase in the corrosion rates in the slightly over-aged condition can be attributed to the decrease in the number density of the precipitates, resulting in an increase in the distance between precipitates and therefore reducing the extent of continuity. Further decrease in the corrosion rates with the increase in the aging time (over-aged and highly over-aged conditions) can be attributed to the change in morphology of the grain boundary precipitates, since there is negligible change in the number density of the precipitates. It can be noted that the grain boundary precipitates in the under-aged as well as the peak-aged conditions are nearly continuous with narrow breaks (Fig. 5a, b, e, f). However, once the samples have been over-aged, the network of precipitates along the grain boundary breaks down heavily for aging temperature of 250 °C (Fig. 5c and d as well as Fig. 5g, h and i) for aging temperature of 330 °C. The extent of this breakdown increases with prolong aging. Even peak aging shows a signature of breaking of continuous network of the grain boundary precipitates (Fig. 5b and f) to a slight extent. However, highly over-aged conditions (Fig. 5d and i) at two different aging temperatures show globularization and growth of the grain boundary precipitates. This probably would allow the grain boundary to face the lesser effect of precipitate free zones in the highly overaged conditions, since the grain boundary precipitates are not continuous as compared to the samples with slightly over-aged conditions. The just overaged condition lies in between the competing factors for the corrosion in the alloy, where the precipitates are losing the continuous features as well as the area of the matrix with depleted Al increases. However, at highly over-aged condition, the effect of globularization of the grain boundary precipitates comes into picture and slight improvement in the corrosion resistance is observed. It should be noted that the Al_8Mn_5 particles have also been reported to affect the corrosion behavior of the alloy [18]. However, their volume fraction and morphologies are not affected at the aging temperatures, i.e., 250 °C and 330 °C. Therefore, the observed changes in the corrosion behavior of the alloy in this study can only be due to the changes

in the morphologies and volume fraction of the $Mg_{17}Al_{12}$ precipitates.

XRD and Raman spectroscopy were performed to analyze the corrosion products formed during the immersion test. XRD was carried out before chemical cleaning of the samples and the patterns are shown in Fig. 9. Peaks corresponding to α-magnesium, $Mg_{17}Al_{12}$ and $Mg(OH)_2$ are clearly visible in the XRD patterns, indicating that the main corrosion product formed during the immersion test is brucite ($Mg(OH)_2$). For better understanding of the peaks, the peak intensity ratio (I/I_{max}) for each condition has been shown in Table 4 following the procedure mentioned in [27, 28]. Several studies have also reported $Mg(OH)_2$ as the predominant corrosion product in the magnesium alloys [14, 29]. Raman spectra (Fig. 10) showed peaks corresponding to both brucite and magnesite ($MgCO_3$). The formation of both brucite and magnesite have also been reported previously [18]. The commonly reported corrosion product in magnesium alloy is brucite, which would form according to the following reactions [14]:

$$Mg \rightarrow Mg^{2+} + 2e^- \text{(anodic reaction)}$$
$$2H_2O + 2e^- \rightarrow H_2 + 2OH^- \text{(cathodic reaction)}$$
$$2Mg^{2+} + 4OH^- \rightarrow Mg(OH)_2 \text{(product formation)}$$

It has been also reported that brucite gets converted to magnesite with time in the presence of CO_2 in the air [29]. In our case, the XRD was performed soon after immersion tests were finished, whereas, the Raman spectroscopy experiments were conducted after few days of immersion tests, which might have resulted in the conversion of brucite to magnesite.
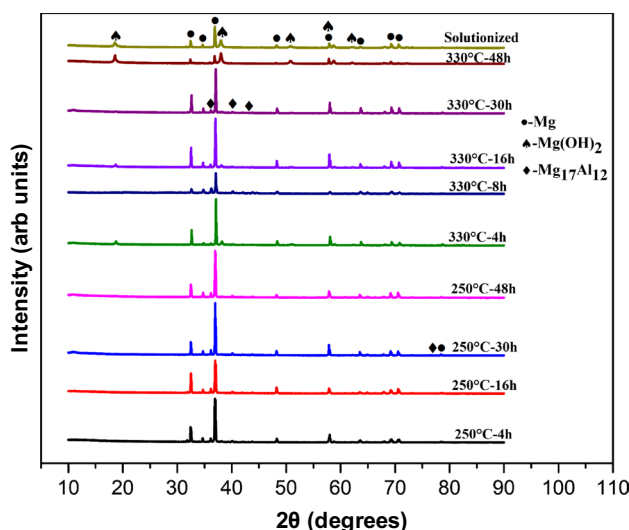

Fig. 9 XRD patterns of samples after immersion tests in a 3.5 wt% NaCl solution

Table 4 The intensity ratios of peaks in aged AZ80 alloy after corrosion (Refer Fig. 9)

| Peaks	2θ	250 °C-4 h	250 °C-16 h	250 °C-30 h	250 °C-48 h	330 °C-4 h	330 °C-8 h	330 °C-16 h	250 °C-30 h	250 °C-48 h	Solutionized
		Peak intensity ratio (I/Imax)									
Mg	32.4	0.17	0.12	0.05	0.07	0.24	0.26	0.06	0.11	0.81	0.31
	34.87	0.03	0.04	0.02	0.04	0.50	0.69	0.04	0.23	0.13	0.05
	36.97	1.00	1.00	1.00	1.00	1.00	1.00	1.00	1.00	0.78	1.00
	48.38	0.05	0.07	0.03	0.02	0.86	0.42	0.09	0.19	0.09	0.08
	57.74	0.05	0.05	0.03	0.05	0.11	0.13	0.02	0.04	0.40	0.07
	63.69	0.04	0.03	0.04	0.04	0.52	0.39	0.04	0.33	0.09	0.06
	69.11	0.06	0.07	0.05	0.08	0.07	0.17	0.01	0.03	0.23	0.06
	70.58	0.05	0.14	0.06	0.09	0.08	0.15	0.02	0.04	0.16	0.15
$Mg_{17}Al_{12}$	36.29	0.04	0.08	0.05	0.06	0.36	0.92	0.03	0.14	0.17	0.05
	40.17	0.04	0.04	0.03	0.03	0.23	0.45	0.03	0.08	0.13	0.04
	43.18	0.01	0.01	0.01	0.01	0.11	0.16	0.01	0.04	0.09	0.03
$Mg(OH)_2$	18.84	0.05	0.04	0.03	0.04	0.78	0.23	0.05	0.13	0.66	0.20
	37.84	0.02	0.02	0.02	0.02	0.29	0.17	0.03	0.06	1.00	0.28
	50.85	0.01	0.01	0.01	0.01	0.19	0.08	0.02	0.03	0.58	0.14
	57.74	0.05	0.05	0.03	0.05	0.11	0.13	0.02	0.04	0.40	0.07
	62.15	0.01	0.01	0.01	0.01	0.11	0.12	0.01	0.03	0.23	0.06
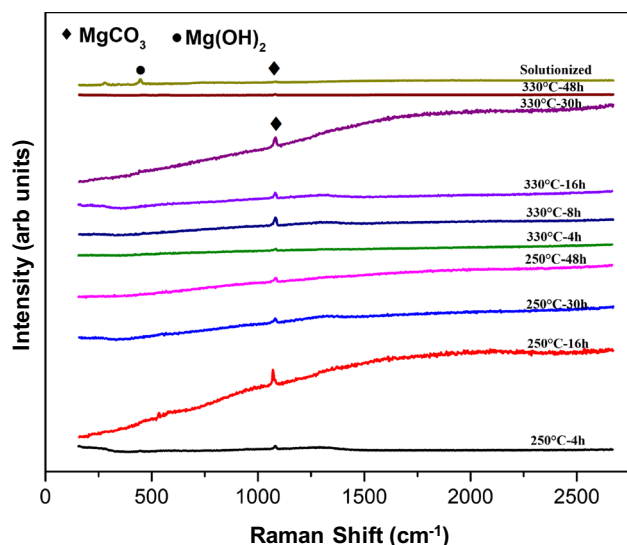
Fig. 10 Raman spectra of samples after immersion tests in a 3.5 wt% NaCl solution

4 Conclusions

The corrosion resistance of the alloy in the aged conditions has been found out to be higher than that of the solutionized condition due to the formation of continuous cathodic $Mg_{17}Al_{12}$ precipitates in the matrix in the aged conditions. Decreasing the aging temperature from 330 °C to 250 °C has increased the corrosion resistance of the alloy, which indicated that the presence of higher number density of cathodic $Mg_{17}Al_{12}$ precipitates dominated over the negative effect of the matrix with the depleted aluminum towards corrosion. Moreover, the peak aged condition at both the temperatures has the higher corrosion resistance than the other conditions due to higher number density and continuous network of cathodic $Mg_{17}Al_{12}$ precipitates. The increase in the corrosion resistance with prolong aging, i.e., highly over-aged conditions were attributed to the size and distribution of the precipitates at the grain boundaries.

Availability of Data and Material (Data Transparency) The data are available from the corresponding author [SSS] upon reasonable request.

Compliance with Ethical Standards

Conflict of interest The authors declare that they have no conflict of interest.

References

1. A.A. Luo, J. Magnes. Alloys. **1**, 2–22 (2013)
2. G.L. Song, *Corrosion Prevention of Magnesium Alloys*, 1st edn. (Woodhead Publishing, Cambridge, 2011), pp. 3–37
3. J.F. Nie, Metall. Mater. Trans. A **43**, 3891–3939 (2012)
4. A. Zindal, J. Jain, R. Prasad, S.S. Singh, Mater. Lett. **201**, 207–210 (2017)
5. A. Zindal, J. Jain, R. Prasad, S.S. Singh, R. Sarvesha, P. Cizek, M.R. Barnett, Mater. Charact. **136**, 175–182 (2018)
6. G. Song, A.L. Bowles, D.H. StJohn, Mat. Sci. Eng. A **366**, 74–86 (2004)
7. M. Fukuzaki, Y. Tamura, N. Kono, J. Jpn. Inst. Light Met. **55**, 389–394 (2005)
8. G. Song, A. Atrens, M. Dargusch, Corros. Sci. **41**, 249–273 (1999)
9. R.K.S. Raman, N. Birbilis, J. Efthimiadis, Corros. Eng. Sci. Tech. **39**, 346–350 (2004)
10. M.-C. Zhao, M. Liu, G. Song, A. Atrens, Corros. Sci. **50**, 1939–1953 (2008)
11. J. Li, Q. Jiang, H. Sun, Y. Li, Corros. Sci. **111**, 299–301 (2016)
12. Y. Dai, X.-H. Chen, T. Yan, A.-T. Tang, D. Zhao, Z. Luo, C.-Q. Liu, R.-J. Cheng, F.-S. Pan, Acta Metall. Sin-Engl. **33**, 225–232 (2020)
13. H.-J. Liao, X.-F. Zhou, H.-Z. Li, M. Deng, X.-P. Lang, R.-M. Liu, T. Nonferr, Metal. Soc. **25**, 3921–3927 (2005)
14. R. Zeng, E. Han, W. Ke, J. Mater. Sci. Technol. **23**, 353–357 (2007)
15. Standard Practice for Preparing, Cleaning, and Evaluating Corrosion Test Specimens, ASTM Standard G1-03
16. Standard Practice for Conventions Applicable to Electrochemical Measurements in Corrosion, ASTM standard G3-14
17. Standard Practice for Calculation of Corrosion Rates and Related Information from Electrochemical Measurements, ASTM G102-89
18. K. Kadali, D. Dubey, R. Sarvesha, H. Kancharla, J. Jain, K. Mondal, S.S. Singh, JOM **71**, 2209–2218 (2019)
19. M.R. Jandaghi, H. Pouraliakbar, Mat. Sci. Eng. A **679**, 493–503 (2017)
20. R. Sarvesha, W. Alam, A. Gokhale, T.S. Guruprasad, S. Bhagavath, S. Karagadde, J. Jain, S.S. Singh, Mat. Sci. Eng. A **759**, 368–379 (2019)
21. R. Sarvesha, Y.L. Chiu, I.P. Jones, S.S. Singh, J. Jain, Mat. Sci. Eng. A **775**, 138973 (2020)
22. Y. Wang, M. Xia, Z. Fan, X. Zhou, G.E. Thompson, Intermetallics **18**, 1683–1689 (2010)
23. G. Zeng, J.W. Xian, C.M. Gourlay, Acta Mater. **153**, 364–376 (2018)
24. K.N. Braszczynska-Malik, J. Alloy. Compd. **477**, 870–876 (2009)
25. S. Yu, S. Gao, C. Liu, X. Han, J. Alloy. Compd. **646**, 431–436 (2015)
26. J.-H. Jun, J. Alloy. Compd. **725**, 237–241 (2017)
27. M.R. Jandaghi, H. Pouraliakbar, A. Saboori, Mater. Res. Express **6**, 1065 (2019)
28. H. Pouraliakbar, M.R. Jandaghi, S.J.M. Baygi, G. Khalaj, J. Alloy. Compd. **696**, 1189–1198 (2017)
29. L. Wang, B. Zhang, T. Shinhara, Mater. Des. **31**, 857–863 (2010)

Publisher's Note Springer Nature remains neutral with regard to jurisdictional claims in published maps and institutional affiliations.